An Adjoint Method for Obtaining the Most Rapidly Growing Perturbation to Oceanic Flows

BRIAN F. FARRELL AND ANDREW M. MOORE*

Department of Earth and Planetary Physics, Division of Applied Sciences, Harvard University, Cambridge, Massachusetts

(Manuscript received 27 December 1990, in final form 10 May 1991)

ABSTRACT

This work explores the formation and growth of waves on oceanic flows using a quasigeostrophic model. In particular, we consider flow regimes consisting of zonal oceanic jets, similar in fact to the westward extension of the Gulf Stream. Traditionally, the formation of waves has been ascribed to exponentially unstable modes, but rather than adopt this paradigm, we seek the most rapidly growing perturbation without restriction of its structure to normal-mode form. Optimal excitations are determined using the adjoint of the quasigeostrophic dynamic equations, and the perturbations found by this method are shown to grow more rapidly than the unstable mode.

Applications of the theory presented here include determination of a tight upper bound on perturbation growth rate, a constructive method for finding the most disruptive disturbance to a given flow, and a method for determining the relative predictability of flows. From the form of the most rapidly growing perturbation, resolution requirements for numerical models can be determined.

1. Introduction

The Gulf Stream is a major source of eddy variance in the Atlantic basin and the formation of waves, meanders, and rings in its westward extension has been intensively studied observationally, analytically, and by numerical simulation (Robinson 1983). Eddies are believed to arise primarily as a result of what is commonly referred to as "instability," a term that distinguishes spontaneous transfer of energy between the stream and perturbations from the influence of wind stress, local heat fluxes, and topographic forcing. We adopt this notion of instability but avoid the more usual identification of instability with exponentially growing normal-mode solutions to linear perturbation equations.

Energy transfer between the stream and perturbations can be separated into two forms, referred to as baroclinic and barotropic. Baroclinic energy is potential energy and arises from density gradients in geostrophic balanced flow; it is associated with depth shear of the current and is released by downgradient perturbation buoyancy fluxes. Barotropic energy is kinetic energy of the stream arising from velocity gradients along density surfaces; it is released by downgradient perturbation momentum fluxes. The Gulf Stream has a jet structure with velocity varying both across the stream and with depth, so that both of these sources of perturbation energy may be important depending on the static stability and the relative strength of the baroclinic and barotropic shear.

Observations reveal rapid growth of meanders in the eastward extension of the Gulf Stream into the North Atlantic basin. Eddy variance associated with these meanders and their finite-amplitude development, resulting in shedding of rings, constitutes a major source of perturbation energy in the ocean. Theoretical understanding of meander growth at small amplitude has traditionally proceeded from the assumption that the stream is unstable to infinitesimal perturbations, and that the growth of exponential modes results in the initial development of meanders (Holland and Haidvogel 1980). However, recent work on the initial-value problem approach to perturbation development has revealed that disturbances of nonmodal form grow much more rapidly than exponential modes over time scales appropriate to observed variance increases in the atmosphere (Farrell 1985, 1989). The assumption underlying this approach is that a spectrum of small, but not infinitesimal, disturbances exists in the flow, and that some subset of this spectrum will be configured favorably to rapidly transform the large source of baroclinic and barotropic energy of the mean jet into perturbation energy. As we cannot, in general, control the form that perturbations take, it is not justified to assume that they initially have the structure of an unstable ex-

* Current affiliation: CSIRO Division of Atmospheric Research, Private Bag No. 1, Mordialloc, Vic. 3195, Australia.

Corresponding author address: Dr. Andrew M. Moore, CSIRO, Division of Atmospheric Research, Private Bag No. 1, Mordialloc Victoria 3195, AUSTRALIA.

ponential mode. If it happened that the most rapidly growing perturbation were of modal form, then the instability problem for small, but finite, perturbations could be understood through study of the eigenvalue problem reduced to identification of the most rapidly growing exponential mode. We show this is not the case and exhibit perturbations that grow more rapidly. Perhaps surprisingly, the perturbation that most effectively excites the most rapidly growing exponential mode itself is not of normal-mode form nor, as it turns out, is it, in general, the fastest growing perturbation we seek.

We study both a barotropic and a baroclinic quasigeostrophic model of a Gulf Stream–like jet and find the most rapidly growing exponental mode on this flow. Having introduced a norm to measure perturbations, we find the optimal excitation for the exponential mode over an appropriate time interval, and the growth of this perturbation is compared to the growth of the exponential mode. Finally, the most rapidly growing perturbation is found and its growth compared with that of the exponential mode and its optimal excitation.

2. Theory of optimal excitation

Before proceeding, we must first decide in what sense we will consider a perturbation to be optimal (i.e., whether the perturbation maximizes the growth rate of perturbation energy, or some other quantity such as squared perturbation streamfunction or perturbation enstrophy). We then need to devise a mathematical tool that will allow us to find the perturbations defined by the growth rate of a given norm. We will show in this section that one way to obtain the optimal excitation for a particular flow regime is to consider the adjoint of the physical system under consideration. The advantage of this approach is that a number of groups (NMC, ECMWF, METEO-France, and AOML, to name a few) are currently developing the adjoints of atmospheric and oceanic general circulation models, which at this stage are mainly for data assimilation purposes. However, as we will demonstrate, these adjoint models have an additional and potentially very powerful application, namely, for the study of instabilities in the atmosphere and ocean, and for investigating the predictability of atmospheric and oceanic forecasting systems.

At this point, a discussion of perturbation equations and the properties of their adjoints is appropriate. The following discussion is by no means exhaustive, and a more extensive discussion can be found in Le Dimet and Talagrand (1986) and Lacarra and Talagrand (1988). Consider a nonlinear system with state vector Ψ:

$$\frac{d\Psi}{dt} = \mathbf{L}(\Psi). \tag{1}$$

The solution $\Psi(t)$ corresponds to a trajectory in phase space uniquely determined by specification of an initial condition $\Psi(t_1)$. Perturbations to this initial condition result in deviations from the original trajectory, so that the system follows a new trajectory $\tilde{\Psi}(t) = \Psi(t) + \psi(t)$. Sufficiently small deviations $\psi(t)$ are obtained by integrating the tangent linear perturbation equation:

$$\frac{d\psi}{dt} = \mathbf{A}(t)\psi, \tag{2}$$

obtained by linearizing (1) about the solution $\Psi(t)$. This system relates deviations from the original trajectory to perturbations $\psi(t_1)$ imposed at the initial time t_1. In general, $\mathbf{A}(t)$ is a linear but nonautonomous operator; it is autonomous if Ψ is a stationary solution of (1). There is a unique operator called the resolvent that connects the initial conditions at time t_1 to the solution at a later time t:

$$\psi(t) = \mathbf{R}(t, t_1)\psi(t_1). \tag{3}$$

Before we can define the adjoint of (3), we must first define an inner product, namely,

$$\langle x, y \rangle. \tag{4}$$

Using this definition of the inner product, we can define a norm that is a measure of the relative magnitude of solutions, that is,

$$|x| = \langle x, x \rangle^{1/2}. \tag{5}$$

The choice of an appropriate inner product and norm is obviously important and should reflect some physically meaningful quantity that will shed light upon a particular aspect of perturbation growth and development. The structure of a normal mode is time invariant; therefore, all of its norms will grow at the same exponential growth rate. In other words, one norm is as good as any other for assessing the growth of such a mode. This, however, is not the case for optimal perturbations. The structure and growth rate of these perturbations depend upon the chosen norm. While unstable exponential modes imply a given structure for a developing disturbance, transient growth arises from a large subset of perturbations that may be the optimal perturbations for many different norms. Therefore, the freedom to choose a particular norm as a measure of perturbation amplitude has physical significance, as discussed in detail by Farrell (1989). We will reserve our choice of inner product and norm appropriate for this study until section 3. For now, our discussion is sufficiently general to encompass any choice of norm and inner product. With this in mind, we will now introduce the concept of an adjoint operator.

For any linear operator $\mathbf{M}$, there exists an adjoint operator $\mathbf{M}^*$, such that,

$$\langle x, \mathbf{M}y \rangle = \langle \mathbf{M}^* x, y \rangle, \tag{6}$$

(Courant and Hilbert 1962, Vol. II). In particular, there exists for the resolvent ($\mathbf{R}$) of our system an adjoint resolvent ($\mathbf{R}^*$) with the property

$$\langle \psi(t), \psi(t) \rangle = \langle \mathbf{R}(t, t_1)\psi(t_1), \mathbf{R}(t, t_1)\psi(t_1) \rangle$$
$$= \langle \mathbf{R}^*(t_1, t)\mathbf{R}(t, t_1)\psi(t_1), \psi(t_1) \rangle, \quad (7)$$

where use has been made of (4). This adjoint resolvent is obtained from $\mathbf{S}(t_1, t)$, the resolvent of the adjoint of (2); that is,

$$\frac{d\psi^*}{dt} = -\mathbf{A}^*(t)\psi^*, \quad (8)$$

where $\mathbf{A}^*(t)$ is the adjoint of $\mathbf{A}(t)$. It is easy to show that the inner product of any solution of the perturbation equation (2) with a solution of the associated adjoint equation (8) is constant, and particularly

$$\langle \psi(t_1), \mathbf{S}(t_1, t)\psi^*(t) \rangle = \langle \mathbf{R}(t, t_1)\psi(t_1), \psi^*(t) \rangle. \quad (9)$$

Recalling the definition of the adjoint (6), inspection of (9) shows that the adjoint of the resolvent of the perturbation equation between t_1 and t is the resolvent of the adjoint equation between t and t_1. Operationally, the perturbation adjoint over a time interval t_1 can be obtained by integrating its adjoint equation backward in time over the same interval.

We are now equipped to find the most rapidly growing perturbation in the norm of the bracket inner product (5) over a specified time interval. We will define a squared amplification factor λ using (5) over a time interval τ as

$$\lambda = \frac{\langle \mathbf{R}(t_1 + \tau, t_1)\psi(t_1), \mathbf{R}(t_1 + \tau, t_1)\psi(t_1) \rangle}{\langle \psi(t_1), \psi(t_1) \rangle}. \quad (10)$$

Equation (10) can be rewritten using the property of the adjoint (6) as,

$$\lambda = \frac{\langle \mathbf{R}^*(t_1, t_1 + \tau)\mathbf{R}(t_1 + \tau, t_1)\psi(t_1), \psi(t_1) \rangle}{\langle \psi(t_1), \psi(t_1) \rangle}. \quad (11)$$

The largest eigenvalue of the composite operator $\mathbf{R}_\tau^*\mathbf{R}_\tau$, where $\mathbf{R}_\tau = \mathbf{R}(t_1 + \tau, t_1)$, will be associated with the most rapidly growing eigenvector of the norm $\langle \psi, \psi \rangle$. The entire spectrum of the operator $\mathbf{R}_\tau^*\mathbf{R}_\tau$ is of interest if we wish to study the growth of variance in the system (Farrell 1990), but for the present purposes we only need the largest λ and its associated eigenfunction. These can be obtained by a simple application of the power method suggested by inspection of (11) (e.g., Booth 1955, p. 85) as follows. First, integrate the first guess $\psi(t_1)$ forward in time from t_1 to $t_1 + \tau$, integrate the result backward in time with the adjoint equation from $t_1 + \tau$ to t_1, and iterate this procedure until convergence to the perturbation of largest λ is isolated. This procedure is constructive in that it provides both the amplification factor $\lambda^{1/2}$ and the most rapidly growing perturbation. Clearly, the form of the adjoint $\mathbf{R}^*$ and the ultimate meaning of the definition of λ resides in our choice of inner product (4). We must, therefore, choose carefully to ensure that we can define a physically meaningful norm.

If we restrict our attention to stationary solutions of (1), the perturbation equation (2) is autonomous and the most rapidly growing exponential mode is easily found by integrating forward a random initial ψ until exponential growth is obtained and the leading eigenfunction emerges. The most effective excitation of the most rapidly growing exponential mode can be found by using the biorthogonality between modes of the perturbation equation and its adjoint. Recalling the property of adjoints (6), and that the spectrum of an operator ν_i is identical to that of its adjoint, a biorthogonality relation can be found (Courant and Hilbert 1962):

$$(\nu_i - \nu_j)\langle \psi_i^*, \psi_j \rangle = 0. \quad (12)$$

An arbitrary initial ϕ can be projected onto the modes:

$$\phi = \sum_{i=1}^{N \to \infty} \alpha_i \psi_i. \quad (13)$$

Excitation of the jth mode, α_j, is found using (12):

$$\alpha_j = \frac{\langle \psi_j^*, \phi \rangle}{\langle \psi_j^*, \psi_j \rangle}. \quad (14)$$

Clearly, in this case the maximum α_j results from choosing ϕ to be the adjoint of the target mode. While for self-adjoint systems the optimal strategy for exciting a mode is to introduce a perturbation with the structure of that mode, this is not the case for nonself-adjoint systems.

3. Description of the quasigeostrophic model and its adjoint

In order to apply the method outlined in the previous section for finding the most rapidly growing perturbation associated with a particular norm, we require the adjoint of the tangent linear system. As mentioned earlier, a number of groups have developed such adjoint models, including the Harvard Oceanography Group (Moore 1991). Given the ready availability of this model, we will use it and the corresponding tangent linear model to explore the growth of instabilities in flow regimes applicable to the Gulf Stream.

The adjoint model of Moore was derived from the finite-element, quasigeostrophic, Harvard Open Ocean Model, which is described in detail by Haidvogel et al. (1980), Miller et al. (1981), and Robinson and Walstad (1987). The nondimensional quasigeostrophic equations of motion for streamfunction (ψ) and vorticity (ζ) are as follows:

$$\frac{\partial \zeta}{\partial t} + \alpha J(\psi, \zeta) + \beta \frac{\partial \psi}{\partial x} = 0 \quad (15)$$

$$\nabla_H^2 \psi + \Gamma^2 \frac{\partial}{\partial z}\left(\sigma \frac{\partial \psi}{\partial z}\right) - \zeta = 0 \quad (16)$$

where

$$J(\psi, \zeta) = \frac{\partial \psi}{\partial x}\frac{\partial \zeta}{\partial y} - \frac{\partial \psi}{\partial y}\frac{\partial \zeta}{\partial x}$$

$$\alpha = \frac{V_0 t_0}{D}; \quad \beta = \beta_0 D t_0; \quad \Gamma^2 = \frac{f_0^2 D^2}{N_0^2 H^2}; \quad \sigma = \frac{N_0^2}{N^2}$$

$$N^2 = \frac{-g}{\rho}\frac{\partial \rho}{\partial z}; \quad f_0 = 2\Omega \sin\Theta_0$$

where V_0, t_0, D, and H are the scalings used for velocity, time, horizontal distance, and height in the vertical, respectively; Θ is the central latitude of the model domain; and Ω is the angular velocity of the earth. The values of these parameters appropriate for the Gulf Stream (see Robinson et al. 1988) are as follows:

$$V_0 = 0.4 \text{ m s}^{-1}, \quad t_0 = 4 \text{ days}, \quad D = 40 \text{ km},$$
$$H = 700 \text{ m}, \quad \Theta_0 = 39.6, \quad N_0^2 = 2 \times 10^{-5} \text{ s}^{-2}$$
$$f_0 = 9.3 \times 10^{-5} \text{ s}^{-1}, \quad \beta_0 = 2 \times 10^{-11} \text{ m s}^{-1}. \quad (17)$$

Note that in the calculations described later, we will neglect the β effect and so $\beta_0 = 0$.

Of interest here is the tangent linear system of (15) and (16) and their adjoints. If we perturb ψ by a small amount $\delta\psi$, and ζ by $\delta\zeta$, the first-order equations describing the evolution of $\delta\psi$ and $\delta\zeta$ are given by

$$\frac{\partial \delta\zeta}{\partial t} + \alpha J(\psi, \delta\zeta) + \alpha J(\delta\psi, \zeta) + \beta \frac{\partial \delta\psi}{\partial x} = 0 \quad (18)$$

$$\nabla_H^2 \delta\psi + \Gamma^2 \frac{\partial}{\partial z}\left(\sigma \frac{\partial \delta\psi}{\partial z}\right) - \delta\zeta = 0. \quad (19)$$

Equations (18) and (19) are discretized in space on an Arakawa B grid (Arakawa and Lamb 1977) with grid spacing 7.5 km and solved numerically using the finite-element method of Fix (1975). The model is discretized in time using an Adams–Bashford scheme and a time step of 22½ min. The model geometry forms a flat-bottomed periodic zonal channel, 600 km in length and 360 km wide. Periodic boundary conditions are imposed upon $\delta\psi$ and $\delta\zeta$ in the east–west direction, and there are solid walls at the northern and southern boundaries.

We can combine (18) and (19) into a single equation for $\delta\psi$, namely,

$$\frac{\partial \delta\psi}{\partial t} + \alpha L^{-1} J(\psi, L\delta\psi) + \alpha L^{-1} J(\delta\psi, L\psi) + \beta L^{-1}\frac{\partial \delta\psi}{\partial x} = 0, \quad (20)$$

where the operator L is defined as

$$L = \nabla_H^2 + \Gamma^2 \frac{\partial}{\partial z}\left(\sigma \frac{\partial}{\partial z}\right). \quad (21)$$

Before we can derive the adjoint of (20), we must choose an inner product that yields a norm suitable for assessing the growth of an instability. To this end we will define

$$\langle \psi, \phi \rangle = -\int\int\int \psi L\phi \, dx dy dz. \quad (22)$$

Consider now,

$$\langle \delta\psi, \delta\psi \rangle = -\int\int\int \delta\psi L \delta\psi \, dx dy dz = -\int\int\int \delta\psi \delta\zeta \, dx dy dz. \quad (23)$$

For constant stratification (i.e., σ constant), the total perturbation energy E of the tangent linear system is given by

$$E = +\frac{1}{2}\langle \delta\psi, \delta\psi \rangle. \quad (24)$$

Therefore, the advantage of using (20) is that it allows us to use the rate of growth of energy norm as a physical measure of perturbation growth.

Using (6) and (7), we can derive the adjoint of equation (20), namely,

$$\frac{\partial \delta\psi^*}{\partial t} + \alpha J(\psi, \delta\psi^*) + \alpha L^{-1} J(\delta\psi^*, L\psi) + \beta L^{-1}\frac{\partial \delta\psi^*}{\partial x} = 0. \quad (25)$$

We can rewrite (25) in the following form,

$$\frac{\partial \delta\psi^*}{\partial t} + \alpha J(\psi, \delta\psi^*) + \mu = 0 \quad (26)$$

$$\nabla_H^2 \mu + \Gamma^2 \frac{\partial}{\partial z}\left(\sigma \frac{\partial \mu}{\partial z}\right) - \alpha J(\delta\psi^*, \zeta) - \beta \frac{\partial \delta\psi^*}{\partial x} = 0. \quad (27)$$

Using (9), it is easy to show that

$$\frac{\partial}{\partial t}\langle \delta\psi^*, \delta\psi \rangle = \frac{\partial}{\partial t}\int\int\int \delta\psi^* \delta\zeta \, dx dy dz = 0. \quad (28)$$

The boundary conditions for the adjoint equations (26) and (27) required to satisfy (6) will depend upon the boundary conditions applied to ψ and ζ when solving the linearized quasigeostrophic equations (18) and (19). Equations (18) and (19) are solved subject to the conditions that $\delta\psi$ and $\delta\zeta$ are periodic in x, $\delta\psi = 0$ at the northern and southern walls, and $\partial\delta\psi/\partial z = 0$ at the top and bottom of the ocean. In order for (6) to be satisfied, we must solve the adjoint equations (26) and (27) subject to the conditions that $\delta\psi^*$ and μ are periodic in x, and $\delta\psi^* = 0$ and $\mu = 0$ at the northern and southern walls, with $\partial\delta\psi^*/\partial z = 0$ at the top and bottom.

In practice, the linearized perturbation equations (18) and (19) are discretized and solved numerically as described earlier. For consistency, therefore, we must derive the adjoint of the discretized versions of (18) and (19). (For further details regarding the derivation of the discretized adjoint model, see Moore 1991.) The discrete analog of (22) is found to be

$$\langle \psi, \phi \rangle = -\sum_i \sum_j \sum_k \psi_{i,j,k} L_{i,j,k} \phi_{i,j,k} \qquad (29)$$

where the subscripts i, j, and k reference model grid points in x, y, and z, respectively. The discrete analog of the time-invariant inner product (28) can also be derived, namely,

$$\sum_i \sum_j \sum_k \delta\psi^*_{i,j,k} \delta\zeta_{i,j,k} = \text{const.} \qquad (30)$$

Following the procedure outlined in section 2, we can use the linearized quasigeostrophic model and its adjoint to find the largest eigenvalue, and associated eigenvector, of the discretized form of the total perturbation energy operator given by (24) for systems with constant stratification. In short, the procedure is as follows: We first integrate (20) forward in time from $t = t_1$ to $t = t_1 + \tau$ starting from some arbitrary first-guess field $\delta\psi(t_1)$. In the examples presented later, the first-guess field is given by a field of random noise. The adjoint model (25) is then run backward in time from $t = t_1 + \tau$ to $t = t_1$ with initial condition $\delta\psi^*(t_1 + \tau) = \delta\psi(t_1 + \tau)$. The linearized quasigeostrophic model (20) is then integrated forward in time once more, subject to the initial condition $\delta\psi(t_1) = \delta\psi^*(t_1)$, and the backward–forward iteration of the adjoint model (25) and linearized model (20) is repeated until the fastest growing eigenfunction emerges in $\delta\psi$. The result given by (30) ensures that the inner product of $\delta\psi^*$ and $\delta\zeta$ remains constant during each iteration.

The background flow field about which (15) and (16) are assumed linearized is a zonal oceanic jet similar in form to that used by Holland and Haidvogel (1980). The horizontal structure of the jet is given by

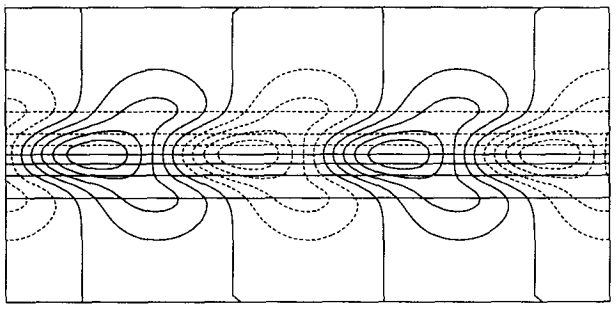

FIG. 1. Streamfunction of the most rapidly growing exponential mode for a zonal barotropic jet. Perturbation streamfunction (with contour interval 0.2) is superimposed on the jet streamfunction (with contour interval 1.0). Dashed contours indicate negative values.

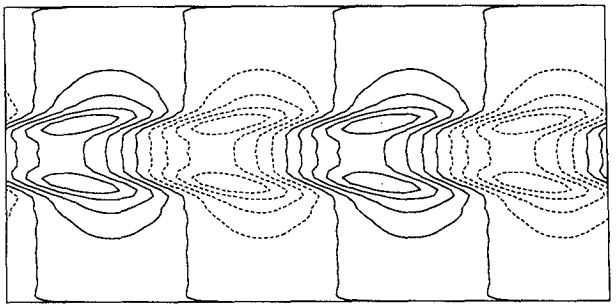

FIG. 2. Streamfunction of the optimal excitation of the most rapidly growing exponential mode on the zonal barotropic jet shown in Fig. 1. Contour interval 0.2.

$$\psi(y) = \frac{-UL\sqrt{\pi}}{2\sqrt{2}} \operatorname{erf}\left(\frac{\sqrt{2}y}{L}\right) \qquad (31)$$

where U is the amplitude of the jet, L is the jet width, and erf( ) is the error function. In all of the experiments described in the next section, $U = 1.6$ m s^{-1} and $L = 56$km, consistent with the Gulf Stream "feature models" used by Robinson et al. (1988). Note, however, that the exponentially growing modes of the system considered here will not necessarily be identical to those of Holland and Haidvogel even with identical flow parameters, because in our system the model domain is periodic, whereas in their model, the domain is bounded on all sides by solid walls.

4. Results and discussion

The Gulf Stream has a jet structure with both baroclinic and barotropic shears, so that conversion from basic-state available potential and kinetic energy to perturbation energy can occur. For simplicity, our first example is restricted to barotropic dynamics by retaining only the first vertical structure mode in (20). In Fig. 1, the basic-state streamfunction is superposed on the most rapidly growing exponential mode obtained by integrating (20) for a sufficient time for the mode to appear. The growth rate is $\omega = 5$, corresponding to 1.25 days per e fold with the nondimensionalization (17). The phase speed is $c_r = 0.12$, corresponding to 63 cm s^{-1}. The structure of this mode is similar to the normal modes found by Holland and Haidvogel (1980). Figure 2 shows the optimal excitation for the mode in Fig. 1 obtained by integrating equation (25). The structure of this optimal excitation for the most rapidly growing exponential mode differs substantially from the structure of the exponential mode itself. Figure 3 shows the evolution of the most rapidly growing perturbation over the time interval $t = 0.25$ corresponding to 1 day, obtained by iterating the dynamic equation and its adjoint 100 times in the manner discussed in section 3. The structure of this most rapidly growing perturbation is clearly different from that of

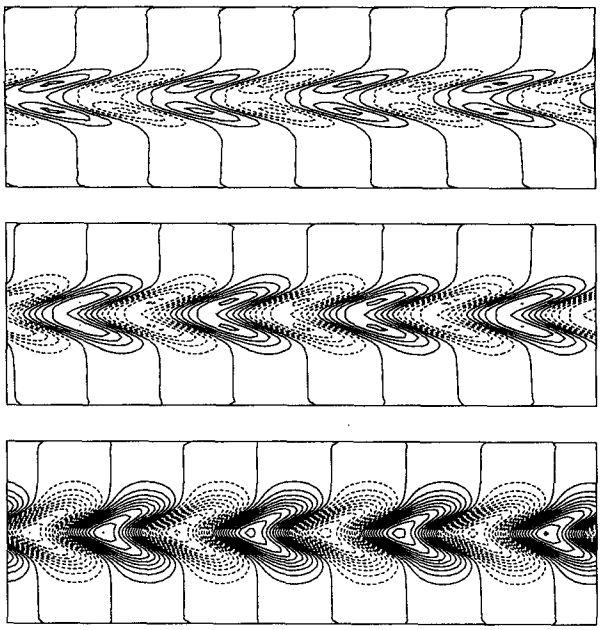

FIG. 3. Streamfunction of the most rapidly growing perturbation over a time interval $t = 0.25$, corresponding to 1 day. The top panel shows the optimal perturbation at $t = 0$ while the middle and bottom panels show the perturbation at $t = 0.125$ and $t = 0.25$, respectively. Contour interval 0.2.

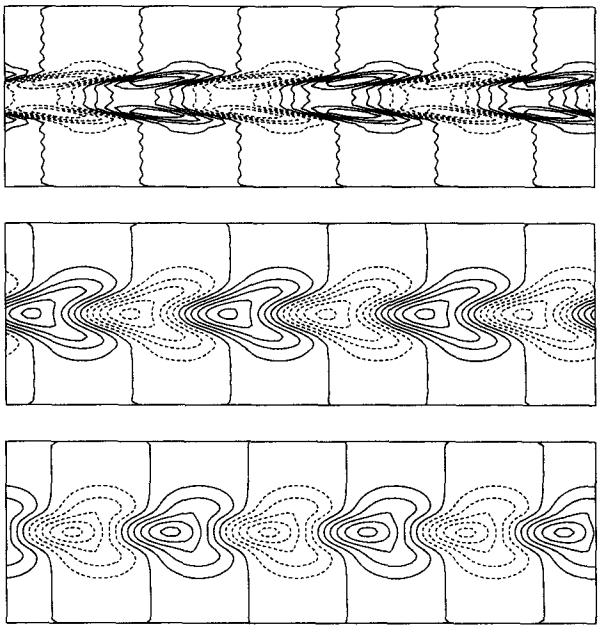

FIG. 5. Streamfunction of the most rapidly growing perturbation over a time interval $t = 1$, corresponding to 4 days. The top panel shows the optimal perturbation at $t = 0$ (with contour interval 0.2) while the middle and bottom panels show the perturbation at $t = 0.5$ (with contour interval = 1.0), and $t = 1.0$ (with contour interval = 5.0), respectively.

both the previous disturbances. In Fig. 4 the growth rate of the perturbation energy is shown for each of the above perturbations as a function of time. The exponential mode grows the least, followed by the optimal excitation, while the most rapidly growing disturbance exceeds both.

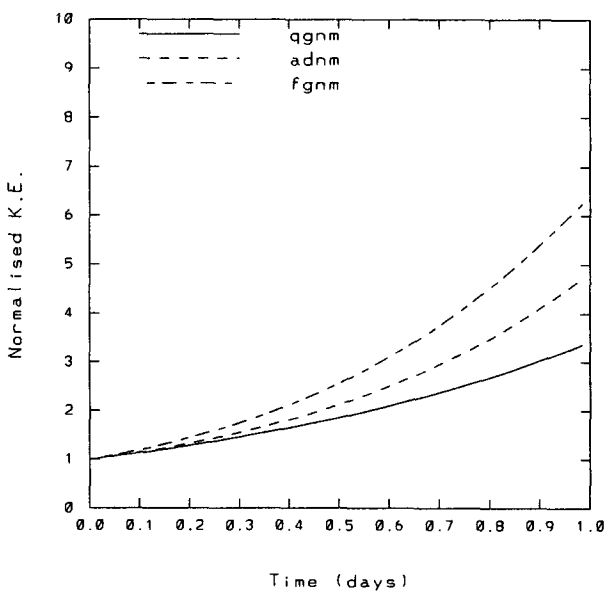

FIG. 4. Normalized perturbation energy growth of the exponential mode (qgnm), the optimal excitation (adnm), and the most rapidly growing perturbation (fgnm) on the zonal barotropic jet.

Figure 5 shows the evolution of the fastest growing perturbation over the time interval $t = 1$, corresponding to 4 days. Compared to the fastest growing perturbation over a 1-day period (Fig. 3), the perturbation of Fig. 5 has increased in wavelength and has a north–south structure similar to that of the optimal excitation shown in Fig. 2. Figure 6 shows the growth rate of the perturbation energy of each perturbation considered above over a 4-day period. Once again, the exponential mode and its optimal excitation are the slowest growing modes.

Our baroclinic example retains two modes in the vertical, with model levels centered at 500 and 3000 m. Velocity and buoyancy frequency profiles are shown in Fig. 7. The horizontal structure of the jet is the same as that of the barotropic jet considered above, and shown in Fig. 1. Even though the jet still has significant horizontal shear, the small value of N^2 ensures that amplitude of barotropic instabilities will be small (e.g., see Holland and Haidvogel 1980). The mode of maximum exponential growth rate has an e-fold time of 0.6 days and a phase speed of 29 cm s^{-1}, and its structure in each model level is shown in Fig. 8. The optimal excitation for this mode is shown in Fig. 9. The most rapidly growing perturbation over 1 day is shown in Fig. 10 after 100 iterations. Again it is seen that the structure of this perturbation differs from the expo-

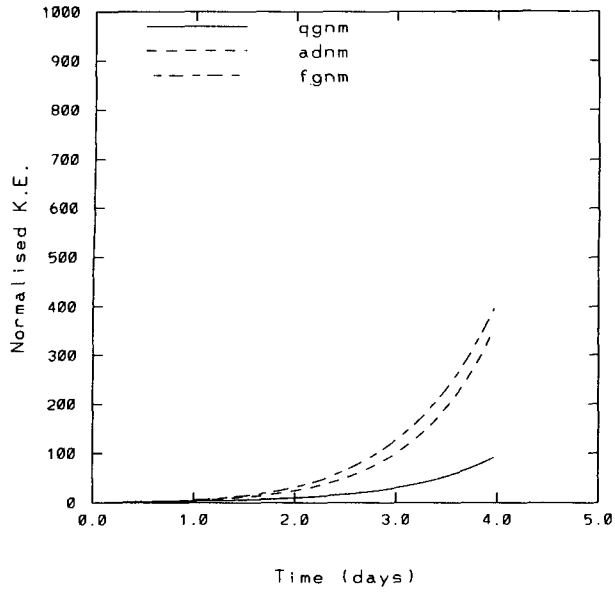

FIG. 6. As Fig. 4 but for a 4-day period.

nential mode and its optimal excitation. The growth of perturbation energy for each perturbation over 1 day is shown in Fig. 11; the most rapidly growing exponential mode again has the smallest growth rate.

The fastest growing perturbation over a 4-day period is shown in Fig. 12. The fastest growing perturbation and the optimal excitation (Fig. 9) are very similar. Figure 13 shows the growth of perturbation energy over a 4-day period for the most rapidly growing exponential mode, its optimal excitation, and the fastest growing perturbation. The curves for the latter two perturbations are indistinguishable. This can be understood if

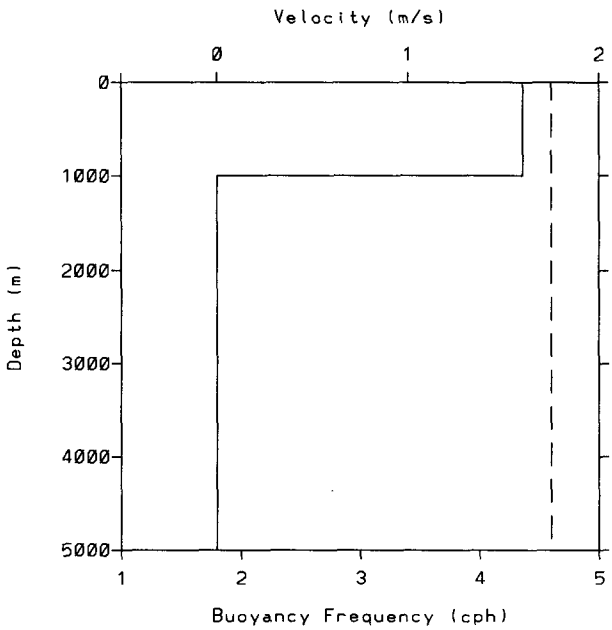

FIG. 7. Velocity profile (solid line) and buoyancy frequency profile (dashed line) for the baroclinic jet of the 2-level model.

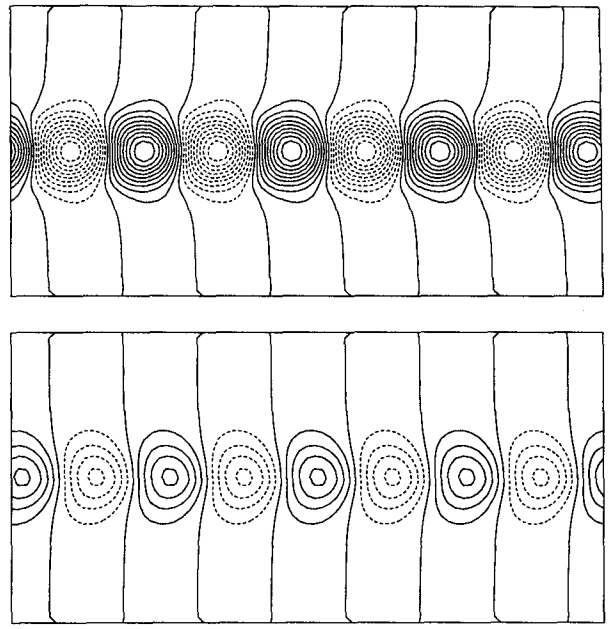

FIG. 8. Streamfunction of the most rapidly growing exponential mode on the zonal baroclinic jet of Fig. 7. The mode is shown at 500 m (top panel) and 3000 m (bottom panel). Contour interval 0.1.

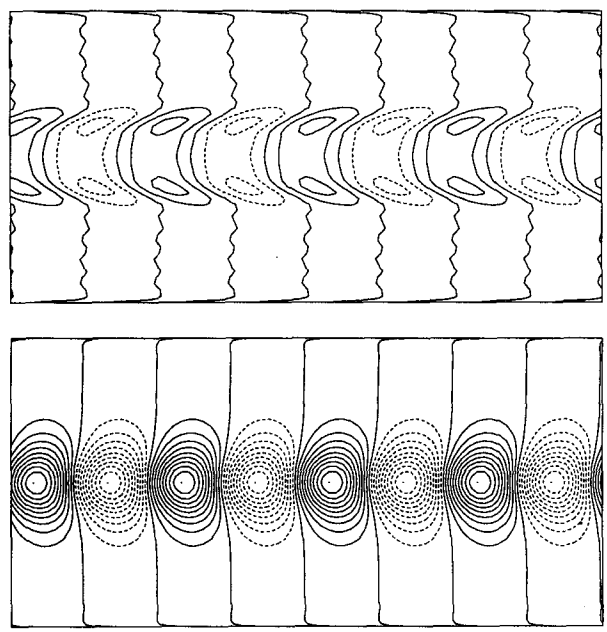

FIG. 9. Streamfunction of the optimal excitation of the most rapidly growing exponential mode on the zonal baroclinic jet of Fig. 7. The mode is shown at 500 m (top panel) and 3000 m (bottom panel). Contour interval 0.1.

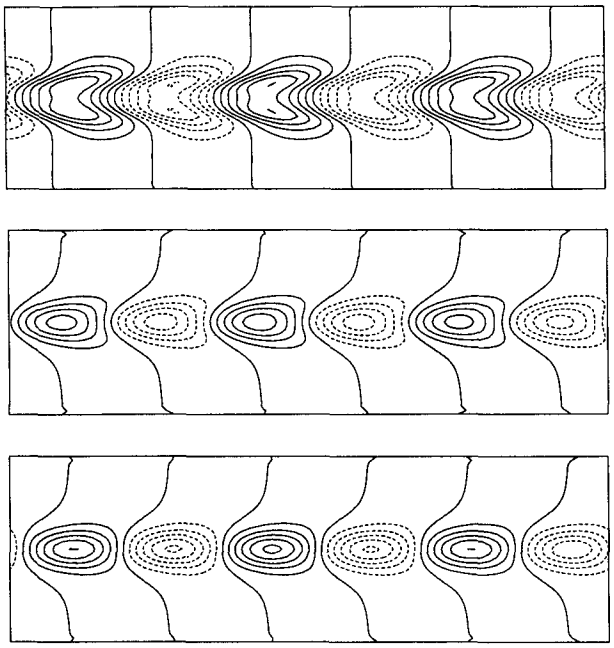

FIG. 10a. Streamfunction at 500 m of the most rapidly growing perturbation on the baroclinic jet of Fig. 7 over a time interval $t = 0.25$, corresponding to 1 day. The top panel shows the optimal perturbation at $t = 0$ (with contour interval 0.2) while the middle and bottom panels show the perturbation at $t = 0.125$ (with contour interval = 1.0) and $t = 0.25$ (with contour interval = 2.0), respectively.

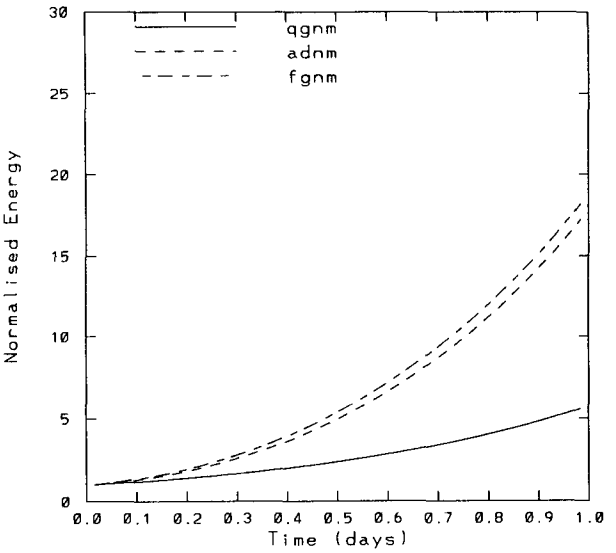

FIG. 11. Normalized perturbation energy growth of the most rapidly growing exponential mode (qgnm), the optimal excitation of the most rapidly growing exponential mode (adnm), and the most rapidly growing perturbation over a time interval $t = 0.25$ corresponding to 1 day (fgnm) on the zonal baroclinic jet of Fig. 7.

we consider that the exponentially growing mode is the fastest growing disturbance over infinite time. Therefore, as the time period of integration of the tangent linear model and the adjoint model is increased,

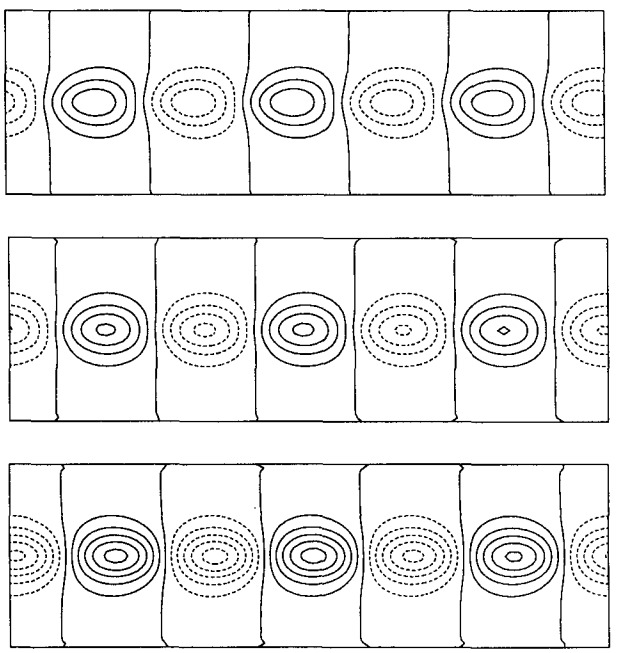

FIG. 10b. As in Fig. 10a, but for the streamfunction at 3000 m. The top panel shows the optimal perturbation at $t = 0$ while the middle and bottom panels show the perturbation at $t = 0.125$ and $t = 0.25$, respectively. The contour interval is 1.0.

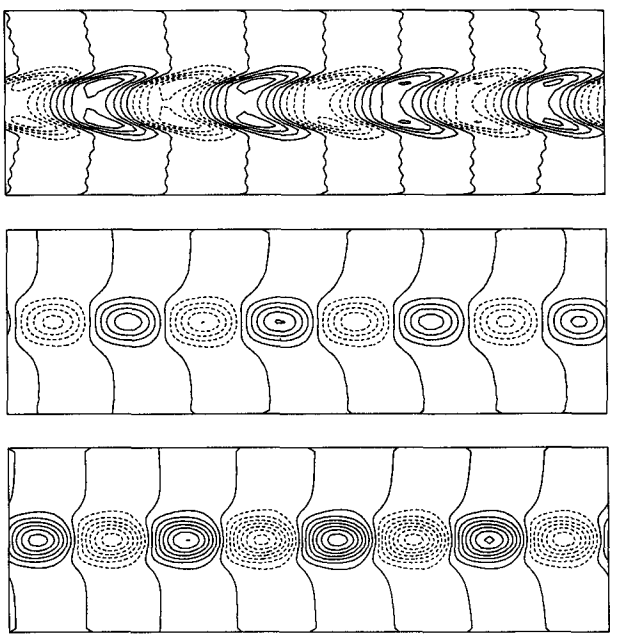

FIG. 12a. Streamfunction at 500 m of the most rapidly growing perturbation on the baroclinic jet of Fig. 7, over a time interval $t = 1$, corresponding to 4 days. The top panel shows the optimal perturbation at $t = 0$ (with contour interval 0.2) while the middle and bottom panels show the perturbation at $t = 0.5$ (with contour interval = 5.0) and $t = 1.0$ (with contour interval = 20.0), respectively.

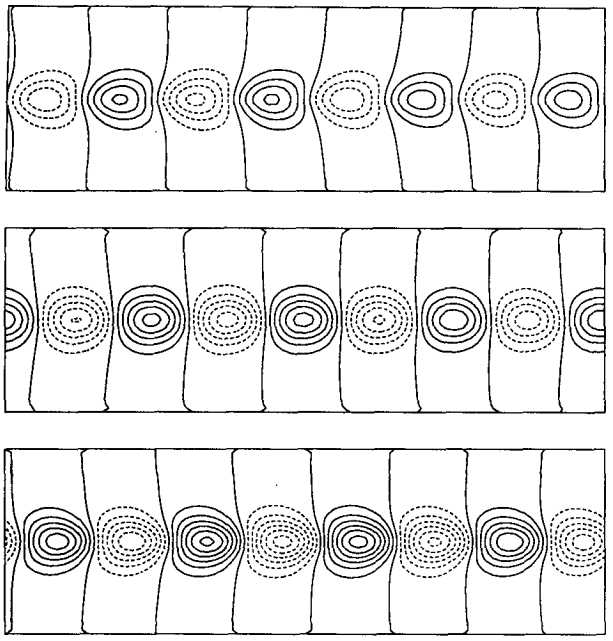

FIG. 12b. As Fig. 12a but for streamfunction at 3000 m. The top panel shows the optimal perturbation at $t = 0$ (with contour interval 1.0) while the middle and bottom panels show the perturbation at $t = 0.5$ (with contour interval = 2.0) and $t = 1.0$ (with contour interval = 10.0), respectively.

the structure of the fastest growing perturbation will approach that of the optimal excitation for the exponential mode.

Finally, we consider an example in which both barotropic and baroclinic instabilities are important. In this case we retain four modes in the vertical, with model levels centered at 150 m, 450 m, 800 m, and 2750 m, and adopt a velocity profile applicable to the Gulf

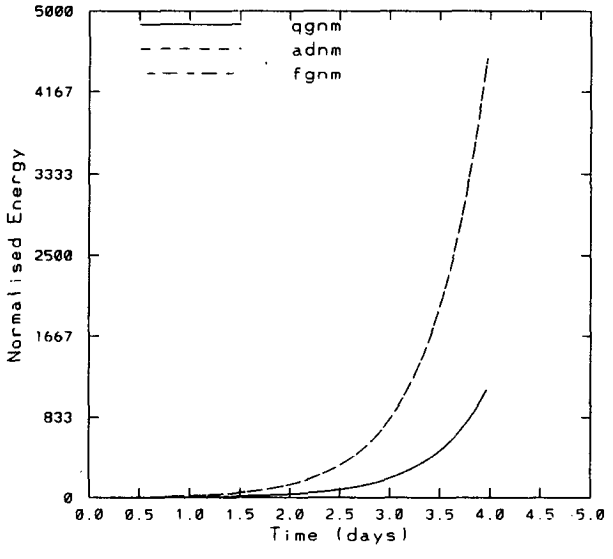

FIG. 13. As Fig. 11 but for a 4-day period.

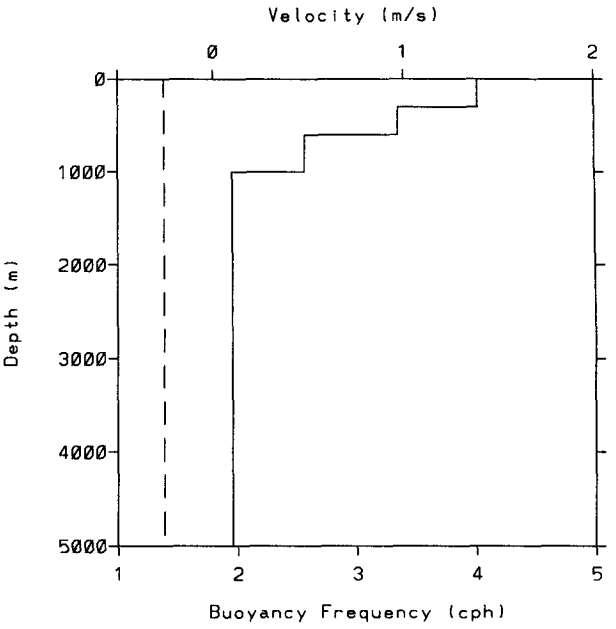

FIG. 14. Velocity profile (solid line) and buoyancy frequency (dashed line) for a four-level jet.

Stream. The velocity and buoyancy profiles for this model are shown in Fig. 14. The horizontal structure of the jet is given by (3.15) and illustrated in Fig. 1.

The exponential mode with a maximum growth rate

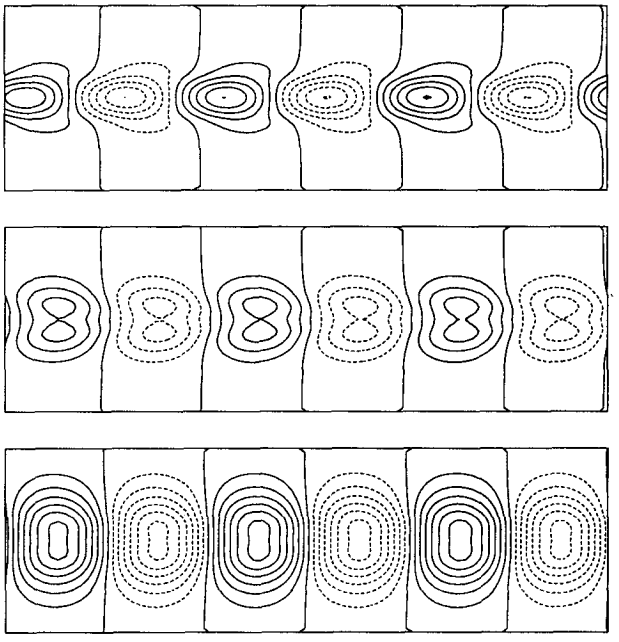

FIG. 15. Streamfunction of the most rapidly growing exponential mode on the zonal jet of Fig. 14. The top panel shows the mode structure at 150 m (with contour interval = 0.2), while the middle and bottom panels show the structure at 800 m (with contour interval = 0.1), and 2750 m (with contour interval = 0.002), respectively.

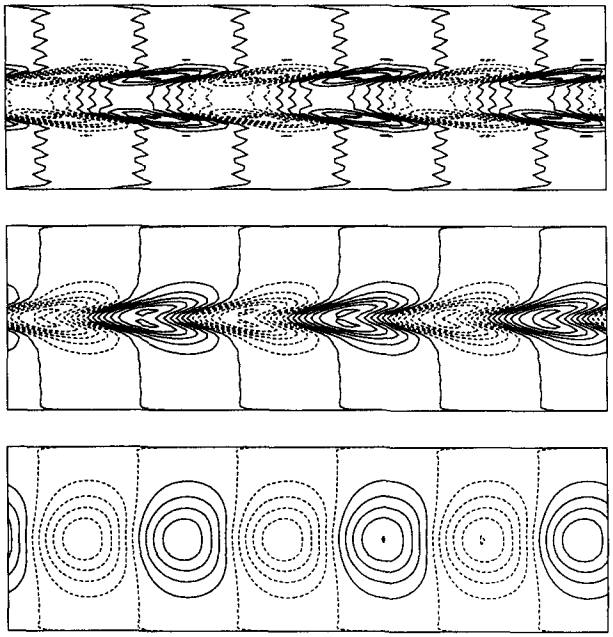

FIG. 16. Streamfunction of the optimal excitation of the most rapidly growing exponential mode on the zonal jet of Fig. 14. The top panel shows the perturbation structure at 150 m (with contour interval = 0.2), while the middle and bottom panels show the structure at 800 m (with contour interval = 0.2), and 2750 m (with contour interval = 0.04), respectively.

has an e-fold time of 1.2 days and a phase speed of 46 cm s^{-1}. Its structure at 150 m, 800 m, and 2750 m is shown in Fig. 15. The optimal excitation for this mode is shown in Fig. 16. The fastest growing perturbation over a period $t = 0.25$ (1 day) is shown in Figs. 17a and 17b. Vertical sections of the streamfunction along the axis of the jet for the exponential mode, its optimal excitation, and for the fastest growing perturbation are shown in Fig. 18. The depth scale in Fig. 18 is stretched so as to highlight the vertical structure of each perturbation in the upper 1000 m. Figures 17 and 18 indicate that the exponential mode with a maximum growth rate is dominated by a baroclinic instability since the streamlines lean backward upstream into the jet flow field in the vertical plane and not in the horizontal plane. Energy is therefore only extracted from the jet flow field through the presence of vertical shear. The fastest growing perturbation on the other hand has both barotropic and baroclinic instability components. Fig. 17a shows that at $t = 0$, the perturbation streamlines lean back into the jet flow field in the horizontal plane, thereby allowing energy to be extracted from the jet through the presence of horizontal shear. In addition, Fig. 18 shows that there is also an upstream tilt in the streamlines in the vertical plane associated with the fastest growing perturbation at $t = 0$. After 1 day ($t = 0.25$) the upstream horizontal tilt and vertical tilt of the streamlines of the fastest growing perturbation has decreased (Figs. 17b and 18). The growth of pertur-

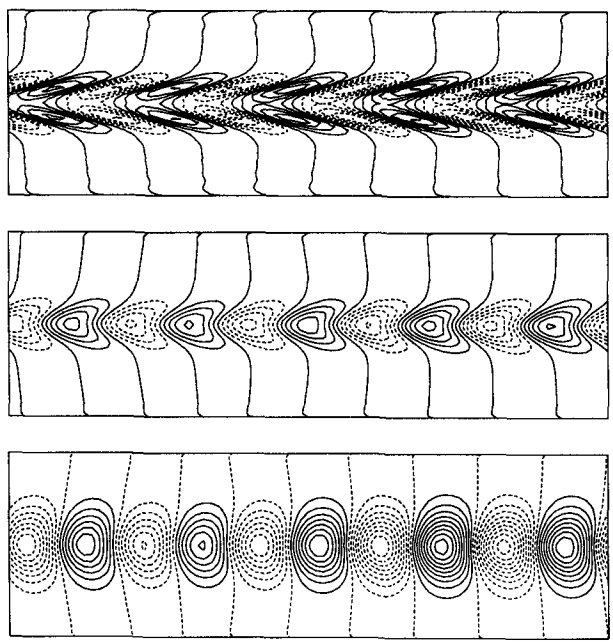

FIG. 17a. Streamfunction at $t = 0$ of the perturbation giving optimal growth over a period $t = 0.25$ (1 day). The top panel shows the perturbation structure at 150 m (with contour interval = 0.2), while the middle and bottom panels show the structure at 800 m (with contour interval = 0.2), and 2750 m (with contour interval = 0.01), respectively.

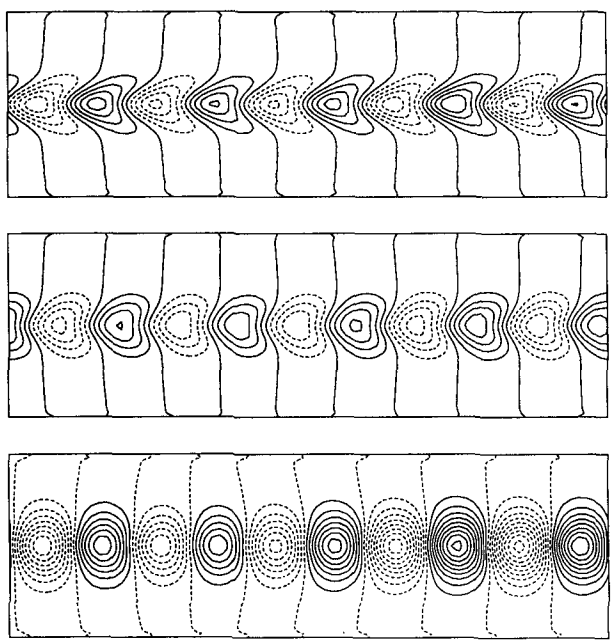

FIG. 17b. As Fig. 17a, but at $t = 0.25$. The top panel shows the perturbation at 150 m (with contour interval = 1.0), while the middle and bottom panels show the structure at 800 m (with contour interval = 0.5), and 2750 m (with contour interval = 0.01), respectively.

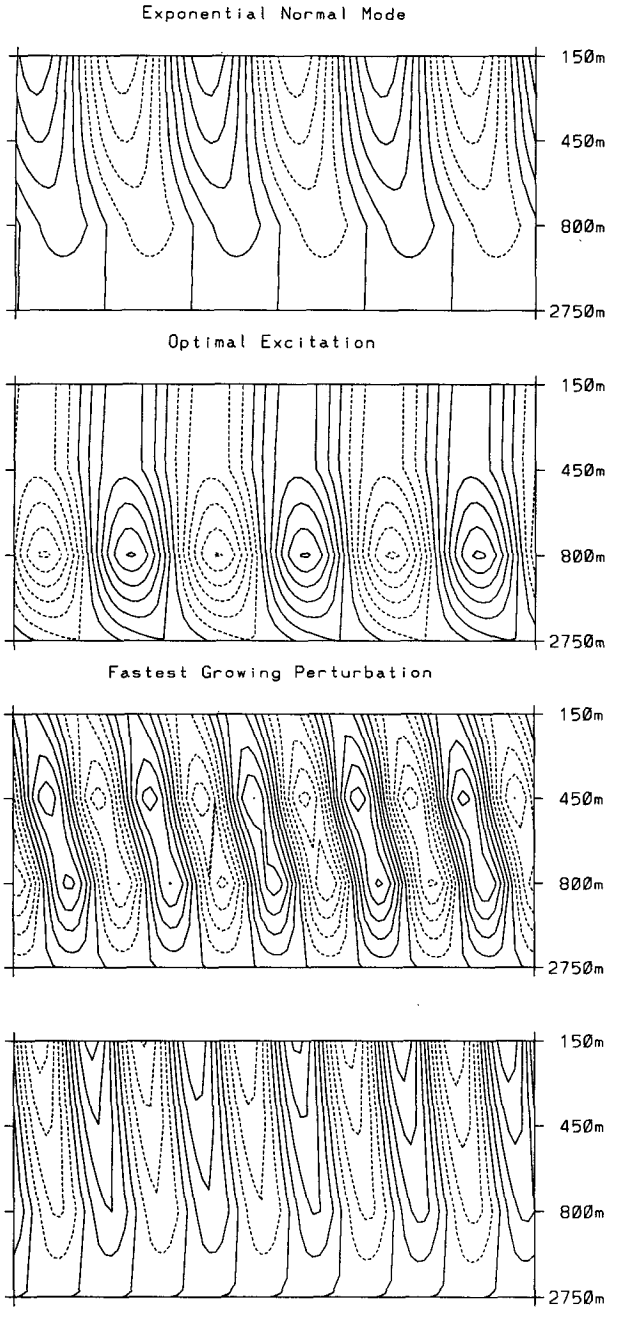

FIG. 18. Vertical sections of streamfunction along the axis of the zonal jet in Fig. 14 for the most rapidly growing exponential mode, (with contour interval = 0.2), its optimal excitation (with contour interval = 0.2), and the fastest growing perturbation which is shown at $t = 0$ (third panel, contour interval = 0.2), and at $t = 0.25$ (fourth panel, contour interval = 1.0).

bation energy for each perturbation on the four-level jet of Fig. 14 is shown in Fig. 19.

5. Conclusions

We have studied the growth of small perturbations in both a barotropic model and a multilevel quasigeostrophic model for a flow regime similar to that of the Gulf Stream and found that the most rapidly growing exponential mode was not the fastest growing perturbation. In fact, the exponential mode was found to be suboptimal even for the task of exciting itself. Solution for the most rapidly growing perturbation over a short limited time interval produced a disturbance that in general differed substantially from both the exponential mode and its optimal excitation. For periods longer than a day or two, the fastest growing mode and optimal excitation are nearly identical for the baroclinic case. Considering that the field of perturbations in the ocean is of finite amplitude and not constrained to assume the form of exponential modes, it is likely that disturbances with structure near to the optimal excitation occur by chance and result in rapid development of meanders.

Our use of stationary basic-state flows is a concession to computational and heuristic convenience, and not a fundamental constraint on the method that can as well integrate the nonautonomous perturbation and adjoint perturbation equations that result from a nonstationary basic-state flow.

It has been observed in the atmosphere that seemingly small changes in the basic-state flow can produce large changes in the optimal excitation growth rate and therefore the predictability of the flow (Palmer 1988). Study of similar situations in the Gulf Stream may reveal flow configurations that are particularly susceptible to the formation of large meanders and subsequent ring generation.

A prediction model that is designed to be valid over a given interval of time should have sufficient hori-

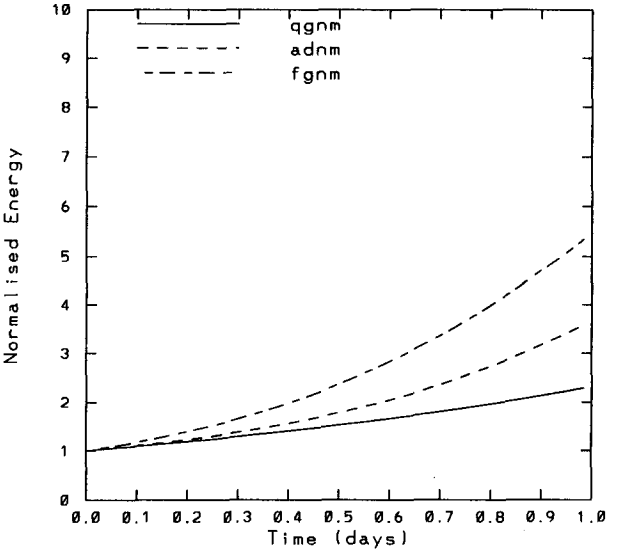

FIG. 19. Normalized perturbation energy growth of the most rapidly growing exponential mode (qgnm), the optimal excitation of the exponential mode (adnm), and the fastest growing perturbation over a time interval $t = 0.25$ corresponding to 1 day (fgnm) on the zonal jet of Fig. 14.

zontal and vertical resolution to capture the structure of the most rapidly growing disturbances. This requirement may be quite restrictive, particularly when the background stratification is weak since, when this is the case, the fastest growing perturbation wavelength is shortest.

Extension of this work to flows with alongstream variation and to flows that vary in time is straightforward. For example, stationary flows with localized jets are found to have optimal excitations that exploit the energy stored in the basic-state deformations associated with confluence and diffluence (Farrell 1990). The increasing availability of adjoints, which are being developed for the purpose of data assimilation in dynamical models, will offer opportunities to extend the study of optimal excitation in the future.

Acknowledgments. This work was supported by NSF ATM-8912432, by the Office of Naval Research under a University Research Initiative Proposal (Grant No. SC 19019), and by supercomputing grants from CRAY Research, Inc. (No. 26615) for computing on a CRAY X-MP/48 located at the National Center for Supercomputing Applications, and a National Allocations Committee (Grant No. NAC16043, HVD 200) for use of a CRAY Y-MP located at the San Diego Supercomputing Center.

REFERENCES

Arakawa, A., and V. R. Lamb, 1977: Computational design of the basic dynamical processes of the UCLA General Circulation Model. *Methods in Comput. Phys.*, **17**, 173–265.

Booth, A. D., 1955: *Numerical Methods.* Butterworth Scientific Publications, 195 pp.

Charney, J. G., R. Fjortoft, and J. von Neumann, 1950: Numerical integrations of the barotropic vorticity equation. *Tellus*, **2**, 237–254.

Courant, R., and D. Hilbert, 1962: *Methods of Mathematical Physics, Vol. 2.* Wiley-Interscience, 830 pp.

Farrell, B. F., 1985: Transient growth of damped baroclinic waves. *J. Atmos. Sci.*, **42**, 2718–2727.

——, 1989: Optimal excitation of baroclinic waves. *J. Atmos. Sci.*, **46**, 1193–1206.

——, 1990: Small error dynamics and the predictability of flows. *J. Atmos. Sci.*, **47**.

Fix, G. J., 1975: Finite element models for ocean circulation problems. *SIAM J. Appl. Math.*, **29**, 371–387.

Haidvogel, D. B., A. R. Robinson, and E. E. Schulman, 1980: The accuracy, efficiency and stability of three numerical models with application to open ocean problems. *J. Comput. Phys.*, **34**, 1–53.

Holland, W. R., and D. B. Haidvogel, 1980: A parameter study of the mixed instability of idealized ocean currents. *Dyn. Atmos. Oceans*, **4**, 185–215.

Lacarra, J., and O. Talagrand, 1988: Short-range evolution of small perturbations in a barotropic model. *Tellus*, **40A**, 81–95.

Le Dimet, F., and O. Talagrand, 1986: Variational algorithms for analysis and assimilation of meteorological observations: Theoretical aspects. *Tellus*, **38A**, 97–110.

Miller, R. N., A. R. Robinson, and D. B. Haidvogel, 1981: A baroclinic quasi-geostrophic open ocean model. *J. Comput. Phys.*, **50**, 38–70.

Moore, A. M., 1991: Data assimilation in a quasigeostrophic open ocean model of the Gulf Stream region using the adjoint method. *J. Phys. Oceanogr.*, **21**, 398–427.

Palmer, T. N., 1988: Medium and extended range predictability and stability of the Pacific. North American mode. *Quart. J. Roy. Met. Soc.*, **114**, 691–713.

Robinson, A. R., 1983: *Eddies in Marine Science.* Springer-Verlag, 609 pp.

——, and L. J. Walstad, 1987: The Harvard open ocean model: calibration and application to dynamical process, forecasting and data assimilation studies. *Applied Numerical Mathematics*, **3**, 89–131.

——, M. A. Spall, and N. Pinardi, 1988: Gulf Stream simulations and the dynamics of ring and meander processes. *J. Phys. Oceanogr.*, **18**, 1811–1853.